Response of the Frog Skin to Steady-State Voltage Clamping

II. *The active pathway*

LAZARO J. MANDEL and PETER F. CURRAN

From the Department of Physiology, Yale University School of Medicine, New Haven, Connecticut 06510. Dr. Mandel's present address is the Department of Physiology, Duke University Medical School, Durham, North Carolina 27707.

ABSTRACT Active Na transport across frog skin was separated from passive Na movement utilizing urea influx as a measure of passive (shunt) permeability. In this manner, the response of the overall active Na transport system to an applied potential was determined over a range from +200 mV to −100 mV. Active Na transport displays saturation as a function of applied potential, and both the level of saturation and the potential at which it is achieved are functions of the Na concentration in the external solution. The saturation with potential appears to involve a different step in the transport process than the saturation of Na flux as a function of external Na concentration. The observations can be qualitatively described by either a one-barrier or two-barrier model of the Na transport system.

INTRODUCTION

In 1951, Ussing and Zerahn (1) demonstrated that in frog skin the measured short-circuit current (SCC) equals net Na transport; under these conditions in which the electrochemical potential of Na is identical in the two bathing solutions, any net Na transport across the skin could be ascribed to active processes. They also observed that the rate of net Na transport decreased with increase in potential difference (PD) across the skin, but could not separate the active from the passive portion of transport at PDs other than zero. Because of this difficulty at nonzero potentials, most subsequent investigators have studied epithelial ionic transport systems under short-circuit conditions. While many properties of transport systems can be investigated in this manner, no information is obtained about their response to an applied potential. Investigations on the effects of applied potential in frog skin and toad bladder demonstrated excitability at high-depolarizing potentials (2, 3) and rectification at high-hyperpolarizing potentials (4, 5). In addition, the

rates of net Na transport and oxygen consumption were observed to increase with increase in depolarizing potential (inside negative) in frog skin (6) and toad bladder (7), suggesting that the rate of active transport was influenced by the applied potential in these epithelia. On the other hand, studies on simpler systems such as squid axon (8) and snail neuron (9) failed to reveal any change in active Na transport as a function of applied potential.

The present investigation involves an attempt to define the detailed response of active Na transport to an applied potential in frog skin. It is based on a previous study (10) demonstrating the effects of steady-state-applied potentials on passive transport through frog skin. Active Na transport can be separated from passive transport utilizing the results of this previous study, resulting in a characterization of the active transport system as a function of potential.

METHODS

General

The experimental methods used were identical to those previously described (10). Briefly, the skin of *Rana pipiens* was mounted as a flat sheet (3.14 cm^2) between Lucite chambers equipped with solution reservoirs (10 ml each) which were stirred and oxygenated with air. The PD across the skin (expressed with reference to the outside solution) was measured with calomel electrodes and current was passed through the skin via Ag-AgCl electrodes. Both pairs of electrodes were connected to the solution reservoirs with agar bridges having a composition identical to that of the bathing solution in the chamber. An automatic voltage clamp that compensated for the resistance of the solution between the PD bridges was used to pass the appropriate current through the skin to maintain a preset PD value. Since solutions with different compositions were often used in the two chambers, the experimental set-up was initially tested for anomalous junction potentials, as described by Frizzell and Schultz (11): the potentials were small under all conditions. Unidirectional fluxes of Na, K, and urea were determined with ^{22}Na, ^{42}K, and [^{14}C]urea as previously described; two flux periods of 15 min duration were measured at each PD after allowing at least 10 min for equilibration at that PD. These transepithelial fluxes from outside to inside solution are denoted "influxes."

Solutions

The composition of solutions used is shown in Table I. The internal solution was always 112 mM NaCl-Ringer (normal Ringer), while the composition of the external solution was varied. In some experiments, the Na concentration was decreased from that of normal Ringer using choline chloride, or a combination of KCl and choline chloride to replace NaCl. In another group of experiments, the NaCl concentration was reduced without substitution, thereby obtaining a hypoosmotic solution. In some experiments, ouabain (10^{-4} M) was added to both solutions. Many of the experiments involved paired skins obtained from the same frog by splitting the skin longitudinally

along back and abdomen to yield two symmetrical pieces. One half of the skin served as a control and was bathed on both sides with normal Ringer throughout the experiment. The other half was first tested in normal Ringer. If the SCC was within 15% of the control, the external solution of the experimental skin was changed to the appropriate experimental solution.

Since the inside solution was always 112 mM NaCl-Ringer, there were frequently ionic concentration differences across the skin. Despite this drawback, there were several reasons why we chose to maintain a constant internal environment. The skin appears to be more sensitive to changes in the composition and osmolarity of the internal than of the external solution (12). Certain external solutions used in the present study such as hypoosmotic solutions and high K solutions are known to have adverse effects on the skin when applied to the inside (12, 13). High concentrations

TABLE I

COMPOSITION OF SOLUTIONS

Solution	Na	K	Choline	Ca	Cl	HCO_3	Tris	Urea
112 mM NaCl-Ringer (Normal Ringer)	112	2.5		1	114	2.5		2
20 mM NaCl-Ringer (Choline replacement)	20	2.5	92	1	114	2.5		2
X mM NaCl-Ringer (Choline replacement)	X	2.5	112-X	1	114	2.5		2
6 mM NaCl-Ringer (Dilute)	6	2.5		1	8	2.5		2
X mM NaCl-Ringer (K replacement)	X	112-X		1	117		3	2
20 mM NaCl+56 mM KCl (Choline replacement)	20	56	36		115		3	2
X mM NaCl+Y mM KCl (Choline replacement)	X	Y	112-X-Y		115		3	2

Concentrations are mM.

of choline chloride and/or low Na on the inside may diminish the rate of transport over the extended periods of time normally required by most of these experiments. In two experiments, skins were first bathed in 4 mM NaCl-Ringer (choline replacement) on both sides and had an average SCC of 1.6 μeq/h cm^2 over 30 min. The *inside* solution was then replaced by 112 mM NaCl-Ringer and SCC *increased* to a steady level of 2.7 μeq/h cm^2 despite the steep Na gradient opposing inward Na transport. When the same experiment was repeated starting with 20 mM NaCl-Ringer, the SCC changes by less than 10%. The presence of even fairly large concentration differences across the skin does not seem a serious problem since the SCC is only 15% higher than net Na transport when 1 mM NaCl is on the outside and normal Ringer is on the inside of frog skin (14).

Calculation of Active Na Flux As a Function of Applied PD

Unidirectional influxes of Na and urea were measured simultaneously as functions of applied potential. The measured Na influx was separated into an active and a passive

(shunt) flux by utilizing the urea influx as a measure of shunt permeability. Mandel and Curran (10) demonstrated that the urea influx was ouabain insensitive and maintained a relationship to the ouabain-insensitive Na influx described by

$$J_{Na}^{i(s)} = \frac{\alpha_{Na} C_{Na}^0}{C_U^0} \left[\frac{-FV/RT}{1 - \exp(FV/RT)} \right] J_U^i, \quad (1)$$

in which $J_{Na}^{i(s)}$ and J_U^i are the Na and urea influxes through the shunt, $\alpha_{Na} = 0.54$ is the ratio of Na to urea permeabilities through the shunt, C_{Na}^0 and C_U^0 are the external Na and urea concentrations, F is the Faraday, V is the applied potential, R is the gas constant, and T is the absolute temperature. Since this relationship was demonstrated with the skin bathed in 112 mM Na, the Na shunt fluxes were calculated from Eq. 1 for this experimental condition, using the measured urea influxes at each potential. The active Na flux $J_{Na}^{i(a)}$, was obtained from the total Na influx, J_{Na}^i, by

$$J_{Na}^{i(a)} = J_{Na}^i - J_{Na}^{i(s)} \quad (2)$$

This procedure is illustrated in Fig. 1, showing a typical experiment (112 mM NaCl-Ringer both sides) in which J_{Na}^i was measured as a function of applied potential and $J_{Na}^{i(s)}$ has been subtracted leaving $J_{Na}^{i(a)}$ as a function of PD. Since the shunt fluxes are ouabain insensitive (10), this procedure is essentially equivalent to taking ouabain-sensitive Na influx as the active component.

The accuracy of the calculation of $J_{Na}^{i(a)}$ depends heavily on the magnitude and

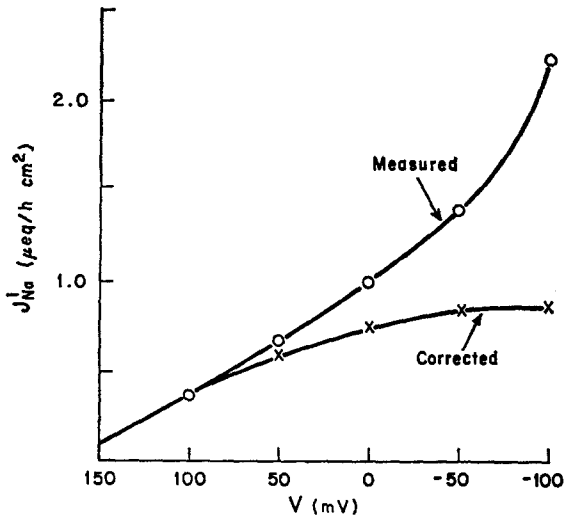

FIGURE 1. Graph of J_{Na}^i vs. PD, illustrating the procedure for calculating $J_{Na}^{i(a)}$. The experimental points in the upper curve are the measured Na influx; the shunt Na flux, calculated from the concurrently measured urea flux (10), is subtracted from the measured flux to obtain the active Na flux (lower curve).

error with which $J_{Na}^{i(s)}$ is determined. If the Na flux through the shunt is a small fraction of the total Na influx, the active component can be accurately determined. However, as $J_{Na}^{i(s)}$ becomes a larger fraction of the total Na influx, the accuracy in the calculation of $J_{Na}^{i(a)}$ decreases. The largest correction for the Na shunt flux occurs at depolarizing potentials in 112 mM NaCl-Ringer; as illustrated in Fig. 1, the correction factor for $J_{Na}^{i(s)}$ is about 50% at −100 mV, 30% at −50 mV, and 15% at short circuit. All skins that required a correction of more than 70% were discarded. The data available for the relationship between $J_{Na}^{i(s)}$ and J_U^i (Fig. 2, reference 10), were utilized for the calculation of $J_{Na}^{i(a)}$ at 0, −50, and −100 mV in 112 mM NaCl-

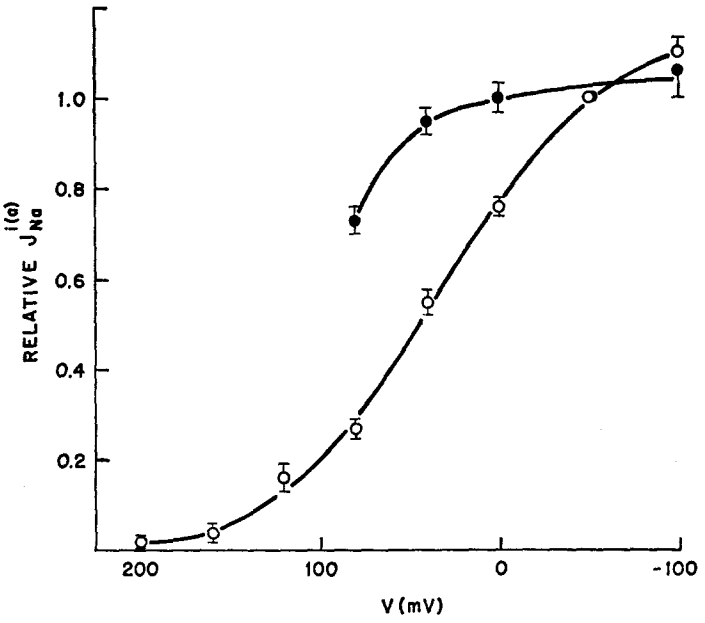

FIGURE 2. Normalized active Na flux vs. PD when both sides are 112 mM NaCl-Ringer. Two populations of experimental points are spontaneously observed. The bars are standard error of the mean. ●, $n = 9$; ○, $n = 39$. The curves were fitted by eye.

Ringer. The accuracy of the calculation of $J_{Na}^{i(a)}$ can be tested at short circuit, since the active Na flux at zero PD should equal the SCC (1). In 49 experiments, the ratio of $J_{Na}^{i(a)}$ at zero PD to SCC was 0.94 ± 0.09 (SEM).

The relationship between ouabain-insensitive Na influx and urea influx described by Eq. 1 was demonstrated in detail only at 112 mM Na. Rather than undertake the extensive study necessary to examine this relationship under the other conditions used, we have employed a simpler procedure. Average ouabain-insensitive Na and urea influxes were measured under the various conditions. $J_{Na}^{i(s)}$ and hence $J_{Na}^{i(a)}$ were then calculated from measured urea influxes using a linear extrapolation from these average values when necessary. The ouabain-insensitive influxes, shown in Table II, were always determined on frogs from the same batch as that used to determine $J_{Na}^{i(a)}$ under the same experimental condition. Although this approach may be less accurate

TABLE II

AVERAGE UNDIRECTIONAL INFLUXES OF NA AND UREA AS A FUNCTION OF APPLIED PD IN OUABAIN-POISONED SKINS WITH DIFFERENT EXTERNAL SOLUTIONS

External solution (mM)	200 mV		160 mV		120 mV		80 mV		40 mV		0		−50 mV		−100 mV	
	$J^{i(s)}_{Na}$	J_U	$J^{i(s)}_{Na}$	J^{i}_{U}	$J^{i(s)}_{Na}$	J^{i}_{U}	$J^{i(s)}_{Na}$	J^{i}_{U}	$J^{i(s)}_{Na}$	J^{i}_{U}	$J^{i(s)}_{Na}$	J^{i}_{U}	$J^{i(s)}_{Na}$	J^{i}_{U}	$J^{i(s)}_{Na}$	J^{i}_{U}
0.5 Na, 111.5 Choline							0.017	0.002 (91%)	0.027	0.002 (69%)	0.046	0.003 (59%)	0.068	0.004 (58%)	0.095	0.007 (58%)
5 Na, 107 Choline							0.016	0.004 (10%)	0.035	0.005 (10%)	0.057	0.006 (9%)	0.097	0.008 (11%)	0.17	0.012 (19%)
8 Na, 104 Choline							0.014	0.003 (5%)	0.034	0.003 (6%)	0.072	0.003 (9%)	0.115	0.005 (11%)	0.175	0.009 (16%)
20 Na, 92 Choline	0.007	0.016 (39%)	0.011	0.014 (24%)	0.015	0.012 (10%)	0.018	0.010 (5%)	0.027	0.010 (5%)	0.130	0.004 (9%)	0.146	0.005 (8%)	0.290	0.006 (13%)
112 Na					0.013	0.005 (6%)	0.031	0.005 (5%)	0.070	0.004 (7%)	0.30	0.007 (16%)	0.70	0.007 (32%)	1.50	0.010 (46%)
55 Na, 55 K							0.029	0.006 (5%)	0.047	0.007 (5%)	0.058	0.007 (5%)	0.125	0.007 (9%)	0.41	0.009 (24%)

Internal solution was 112 mM NaCl-Ringer. Each value is average of four experiments. Fluxes are given in μeq/h cm^2 (J^i_{Na}) or μmol/h cm^2 (J^i_U). Numbers in parentheses are the average percentages of the measured Na influx under the respective *unpoisoned* conditions.

than the one used at 112 mM Na, it is justified by the fact that all the shunt fluxes (except those at 0.5 mM Na) are a relatively small fraction of total influx (see Table II).

RESULTS

Effect of Applied PD on Active Na Flux

As shown in Fig. 2, the active Na influx displays an S-shaped characteristic as a function of applied PD when both sides of the skin are bathed with 112 mM NaCl-Ringer. The data are normalized to the flux observed at −50 mV. Two distinct populations with significantly different behavior were observed. One group (nine skins) appears to achieve saturation of Na transport at a PD close to the average open-circuit potential (about 30 mV); in the other group (40 skins), saturation appears to occur at more negative PDs and is less clearly demonstrated because of the relatively larger error in $J_{Na}^{i(a)}$ at −100 mV (see Methods). The average magnitude of $J_{Na}^{i(a)}$ at the normalizing potential was 1.36 ± 0.2 μeq/h cm² for the smaller group and 1.26 ± 0.1 μeq/h cm² for the larger group. These fluxes do not differ significantly, indicating that the main difference between the two groups is the PD at which saturation occurs. The data for the lower curve were obtained in two stages to insure the viability of the skin at all PDs (a single experiment covering the full range of PDs would have lasted 6 h, with questionable results after the first 3 h). One stage covered the PDs from 200 to 40 mV and the other covered 80 to −100 mV with overlap at 40 and 80 mV. The left part of the curve was normalized to the averages of the right part at both overlap potentials.

Effect of External Na Concentration

The active Na influx vs. PD was calculated at various external Na concentrations. These results can, however, be better understood by referring initially to Fig. 3, curve *a*, which shows the saturation of SCC (active Na transport at zero PD)[1] as the external Na concentration is increased. This behavior of the SCC is the same as that described by Cereijido et al. (15) for experiments in which the Na concentrations on both sides of the skin were identical. In experiments shown in curve *a*, half saturation is achieved at 5 mM NaCl, and the SCC at 20 mM is not significantly different from that at 112 mM NaCl. The steepness of these curves appears to vary with different batches of frogs; in some cases, half saturation could be reached at NaCl concentrations as low as 2 mM.

If the results of Fig. 3 (*a*) were replotted on a graph of $J_{Na}^{i(a)}$ vs. PD (Fig. 2),

[1] SCC cannot be precisely equated with active Na transport under these conditions because there is a Na concentration difference across the membrane. However, the results of Biber et al. (14) suggest that the discrepancy should be small.

a one-dimensional saturation would be observed on the vertical line at zero PD as the external NaCl concentration is increased. The point at 20 mM NaCl would be indistinguishable from the one at 112 mM NaCl and, depending on the steepness of the saturation curve, lower concentrations may also be indistinguishable from 112 mM NaCl. With this background, it is easier to understand that, at all measured PDs, experimental points for external NaCl concentrations of 112 mM, 20 mM, and 8 mM NaCl are essentially identical to each other as shown in Fig. 4. At lower external NaCl concentrations, the general S-shape of the curve is preserved with a lower saturation level for the active flux. All of the experimental points shown in Fig. 4 were obtained from

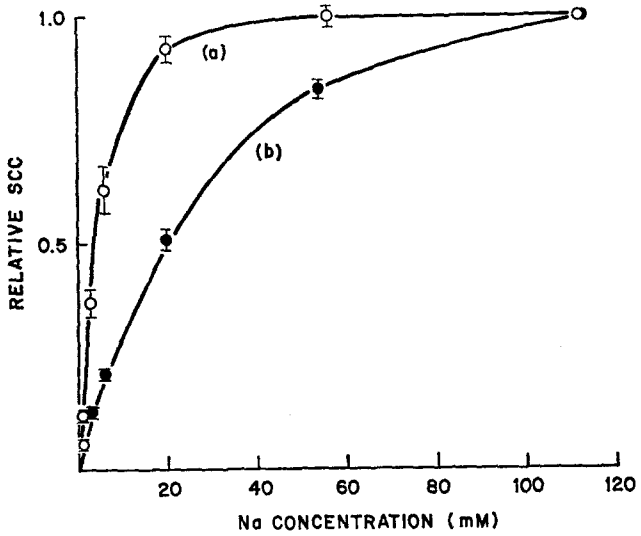

FIGURE 3. Short-circuit current as a function of external Na concentration. curve *a*: choline replacement ($n = 6$); curve *b*: K replacement ($n = 6$).

matched halves of the same skin, one used to measure active Na fluxes at 112 mM NaCl (control) and the other at a lower NaCl concentration. Thus, the data at each concentration were obtained in a different group of skins, each with its own controls; the control group shown in Fig. 4 was pooled from all these measurements. The data are normalized, as in Fig. 2, at -50 mV for the control group; the results for lower NaCl concentrations were each normalized to their respective paired controls.

In Fig. 4, the curves at 6 mM NaCl and higher concentrations appear to be approaching saturation at high-depolarizing potentials, without attaining it at -100 mV. Experimental points at higher PDs (more negative) should determine whether saturation is reached or not; however, at higher PDs, the shunt permeability increases rapidly in the isotonic external solutions used for these experiments (10), leading to a large error in the calculation of $J_{Na}^{i(a)}$.

Dilute external NaCl solutions could be used to experiment at higher negative PDs, since the shunt permeability under those conditions is lower (10). A group of four experiments was performed in matched skins to test for any differences in $J_{Na}^{i(a)}$ vs. PD between external isotonic 6 mM NaCl-Ringer (choline replacement) and dilute 6 mM NaCl-Ringer. The results, shown in Table III, indicate identical rates of active transport at 0, −50, and −100 mV. Thus, dilute 5 mM NaCl-Ringer was used to examine $J_{Na}^{i(a)}$ vs. PD over the range 0 to −200 mV with results shown in Fig. 5. The saturation, which is suggested between 0 and −100 mV, becomes more clearly defined at −200 mV. This result, together with the clear saturation observed at lower external

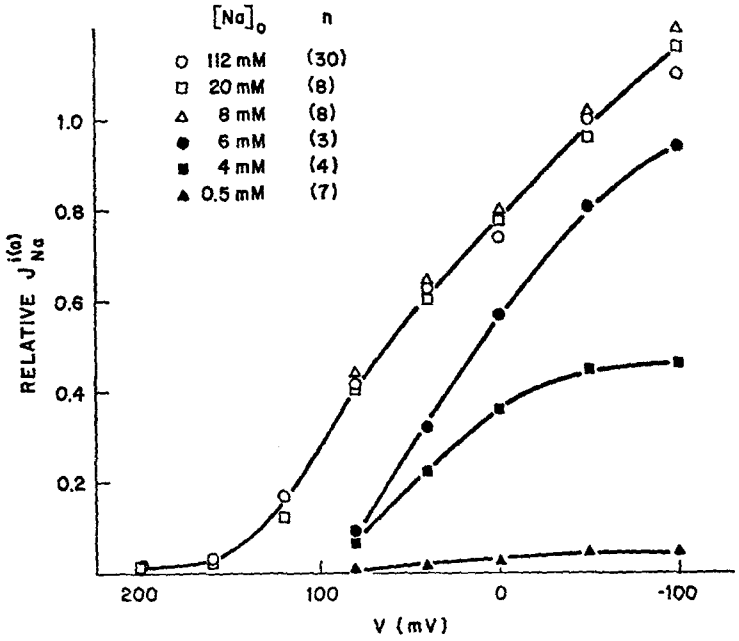

FIGURE 4. Active Na influx (normalized) vs. applied potential at seven external Na concentrations (choline replacement). Standard errors are about the same as in Fig. 2; they have been omitted for clarity.

TABLE III

EFFECT OF EXTERNAL CHOLINE REPLACEMENT ON $J_{Na}^{i(a)}$ VS. PD AT 6 mM NaCl (n = 4)

	0	−50 mV	−100 mV
$J_{Na}^{i(a)}$ dilute (μeq/h cm²)	0.46±0.07	0.66±0.07	0.80±0.06
$J_{Na}^{i(a)}$ choline (μeq/h cm²)	0.46±0.88	0.64±0.09	0.75±0.13

NaCl concentrations and the spontaneous saturation observed in 20% of the skins tested (Fig. 2), suggests that saturation with PD is a real property of the active Na transport system. The PD at which saturation is reached appears to be variable, and the magnitude of the saturated active flux depends on the external Na concentration.

Na Transport Kinetics

The active transport of Na saturates as a function of external Na concentration (Fig. 3) and as a function of applied PD (Figs. 2, 4, and 5). Two sets of experiments were performed to test the interrelationship between these two effects.

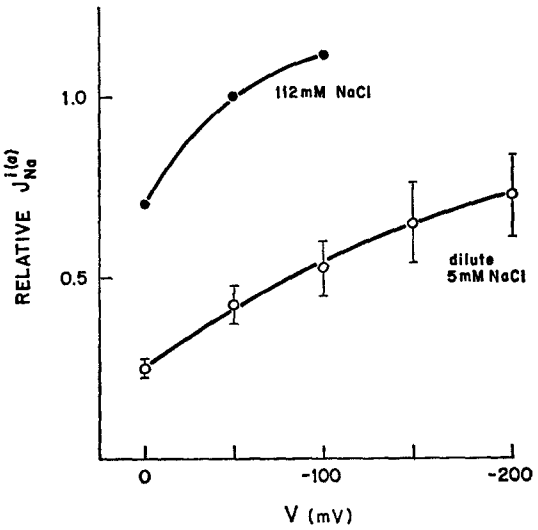

FIGURE 5. Active Na influx (normalized) vs. applied potential over the range 0 to −200 mV to demonstrate saturation at higher PD. Control vs. 5 mM NaCl-Ringer (dilute); $n = 4$.

In one series, SCC and $J_{Na}^{i(a)}$ at 50 mV were measured on the *same* skins as functions of external NaCl concentration. In the other series, SCC and $J_{Na}^{i(a)}$ were measured at −50 mV. Results are shown in Fig. 6 in terms of double reciprocal plots. The straight lines obtained indicate a hyperbolic relationship between the two variables that can be interpreted in terms of Michaelis-Menten kinetics. In both cases, the intercepts on the ordinate are significantly different from each other, indicating that the maximum transport rate (saturation level) is decreased (from 1.7 to 0.7 μq/h cm^2) at 50 mV and is increased (from 1.0 to 1.5 μeq/h cm^2) at −50 mV when compared to the rate at zero PD. The intercepts on the abscissa are identical in Fig. 6 *b* but are different in Fig. 6 *a*, suggesting that the half-saturation concentration (K_t) is unchanged between 50 mV and 0 but decreases between 0 and −50

mV. These results indicate that the interaction between the external Na concentration and applied PD is of a noncompetitive or uncompetitive nature, suggesting actions on different steps in the transport process.

Effect of External K on $J_{Na}^{i(a)}$

As indicated in Fig. 3, equimolar replacement of KCl for NaCl in the external solution inhibits the SCC compared to results obtained with choline chloride

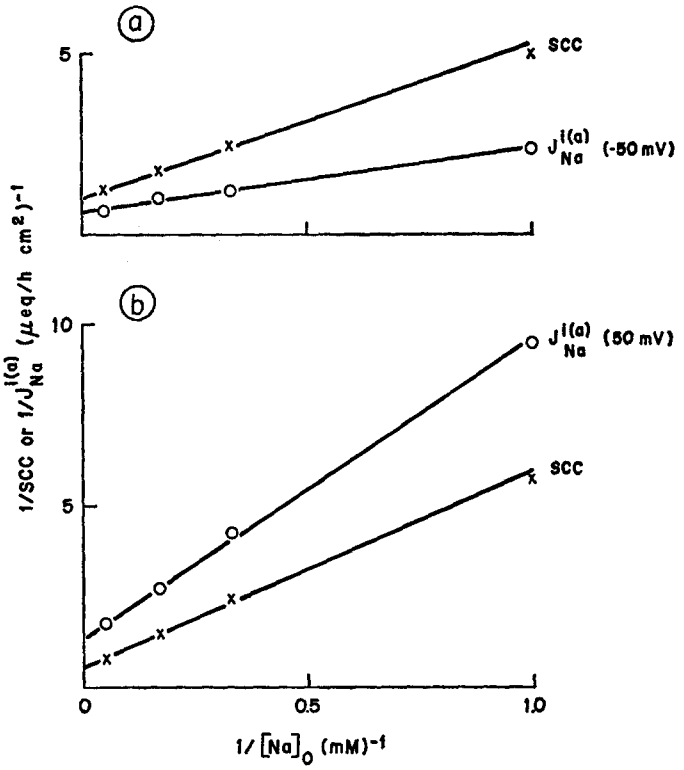

FIGURE 6. (*a*) Plot of reciprocal of SCC or $J_{Na}^{i(a)}$ at −50 mV vs. reciprocal of external Na concentration. (n = 6). (*b*) Plot of reciprocal of SCC or $J_{Na}^{i(a)}$ at 50 mV vs. reciprocal of external Na concentration. (n = 4). Regression lines were calculated by the least-squares method.

replacement. In the presence of KCl, the SCC is still nearly equal to active Na transport; in six experiments with an external solution of 20 mM NaCl + 92 mM KCl the ratio of $J_{Na}^{i(a)}$ at PD = 0 to SCC was 0.84 ± 0.04. The remaining 16% of the current is probably due to net K influx through the shunt down its concentration gradient. K influxes measured with ^{42}K were low, and agreed well with influxes obtained at the same external KCl concentration in ouabain-poisoned skins (10), suggesting passive movement through the shunt pathway.

More systematic experiments were performed by measuring SCC as a function of external NaCl concentration at various fixed external KCl concentrations using choline chloride to maintain constant ionic strength (see Table I for exact solution compositions). The results of a typical experiment are shown in Fig. 7 in terms of a double reciprocal plot. The regression lines for all three K concentrations have a common intercept on the ordinate, indicating that K acts as a competitive inhibitor of Na transport. The value of K_t changes from 3 mM when $[K]_0 = 3$ mM to 10 mM when $[K]_0 = 56$ mM.

The effect of external KCl on the relationship between active Na transport and PD was determined with results shown in Fig. 8. The experiments at

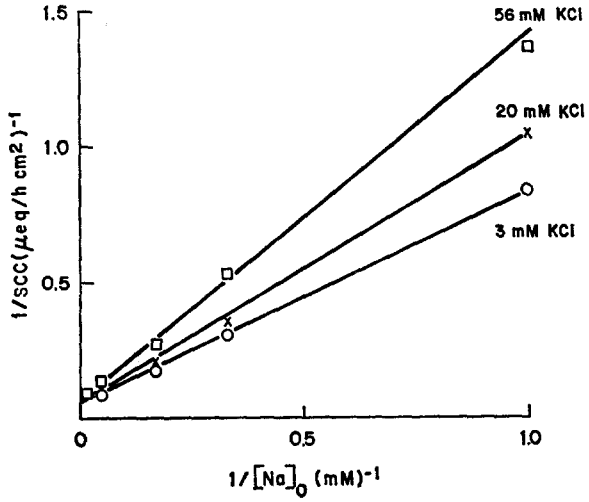

FIGURE 7. Reciprocal of normalized SCC vs. reciprocal of external Na concentration at three external K concentrations for a typical experiment. Regression lines were calculated by the least-squares method.

20 mM NaCl + 92 mM KCl in the external solution show significant inhibition of $J_{Na}^{i(a)}$ compared to paired controls. The experiments at 56 mM NaCl + 56 mM KCl show much less inhibition, as expected from the results shown in Fig. 7. Both curves obtained at high external K concentrations are indistinguishable from those obtained in the lower concentration NaCl-Ringer shown in Fig. 4, suggesting that the PD acts on a locus separate from that of the Na-K competition.

Reversibility of Active Na Transport

In experiments covering such a wide range of PDs and lasting about 3 h each, the reversibility of the skins after being exposed to such an experimental regime must be considered. Skins exposed to potentials in the range 100 to −50 mV recovered their initial SCC and open-circuit potential rapidly, even

after being exposed to those PDs for hours. Complete recovery of the skins was essential to perform the experiments depicted in Fig. 6, since the skins were alternated between short circuit and either 50 mV or −50 mV. Recovery from −100 mV was variable, and was a function of time but not of external NaCl concentration; most skins exposed to this PD for 40 min returned to about one-half the original SCC. Recovery from high-hyperpolarizing potentials was also variable, with the skins returning to 50–80% of the original SCC.

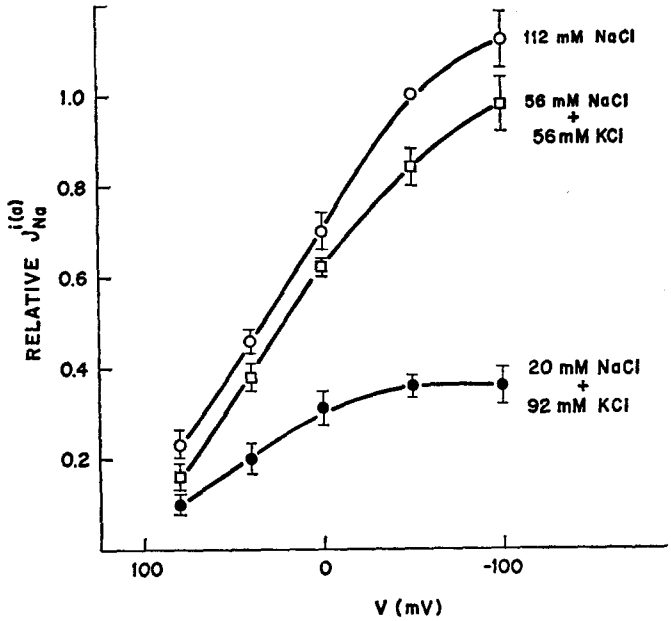

FIGURE 8. Active Na influx (normalized) vs. applied potential testing the effects of external K concentration. Control vs. 56 mM NaCl + 56 mM KCl (n = 3), and control vs. 20 mM NaCl + 92 mM KCl (n = 6).

DISCUSSION

The present results indicate that active Na transport is a saturable function of applied PD (Figs. 2, 4, and 5) as well as of external Na concentration (Fig. 3). The data in Fig. 6 suggest a degree of independence between these two factors, since an applied PD alters the maximal transport rate that can be achieved as a function of external Na concentration. This observation implies that Na concentration and PD may act on separate steps of the overall transport system. On the other hand, external K seems to compete directly with external Na for the same sites of the active Na pathway. These observations may provide some indication of the possible sequence of steps involved in active Na transport in frog skin.

Various factors must be considered in interpreting the observed saturation of active Na transport with PD. First, unstirred layers at the membrane solution boundaries do not appear to influence significantly the saturation under the conditions used in most of these experiments. An unstirred layer on the external surface of the skin does not play a significant role in determining active Na transport since $J_{Na}^{i(a)}$ is unaffected by large changes in external ionic strength as shown in Table III. When unstirred layers are rate determining, changes in ionic strength should cause appreciable alterations in the behavior of the system under conditions similar to those studied here (16, 17). An unstirred layer at the inner surface of the epithelium would be expected to exert a larger effect (slowing transport) at high rates of transport than at low rates due to accumulation of Na adjacent to the internal surface. Since the shape of the curves relating $J_{Na}^{i(a)}$ to PD are qualitatively similar at all external Na concentrations, regardless of the actual magnitude of Na flux, a major effect of an unstirred layer at the inner surface seems unlikely. Thus, the effective permeability of the skin to Na appears to be sufficiently low to minimize effects of unstirred layers. Second, saturation could occur as a result of damage to the skin caused by high depolarizing PDs. As indicated in the Results section, recovery from depolarizing PDs of -100 mV or higher is often not complete. However, the Na transport measured at -100 mV is probably still accurate because it displays characteristics similar to those observed in the 20% of skins showing saturation at lower PDs (Fig. 2). Third, as PD is increased in the depolarizing direction, its distribution may be altered in such a way that the actual PD appearing across the rate-determining step of Na transport may remain approximately constant even though overall PD increases. Thus, the saturation of Na flux with PD would be apparent only. Such an explanation seems unlikely in view of the fact that some skins display saturation in the region of zero PD. Also, in previous studies (10) on the shunt pathway, there was no evidence for such alterations in the distribution of depolarizing PDs, at least up to -100 mV. Thus although we cannot completely rule out these explanations, they are somewhat unlikely and it seems reasonable to conclude that saturation of $J_{Na}^{i(a)}$ with PD is a property of the active Na transport system.

The site of action of the applied potential is difficult to ascertain in the absence of microelectrode measurements to establish the distribution of PD through the epithelium, and even that information might be inadequate to explain the observed effects fully. Certain inferences can, however, be made from the data, especially with reference to the Na transport model proposed by Koefoed-Johnsen and Ussing (18). In this model, the first step involves passive diffusion of Na from the external solution into the transporting cells, followed by a second step of active extrusion of Na into the serosal solution in exchange for K in electroneutral fashion. If both of these postulated proc-

esses occur in the same cells, as suggested by later modifications of the theory (19), the amount of Na actively transported would depend on the Na concentration in the cells. The saturation of Na transport as a function of external Na concentration would be attributed to the saturation of the active transport step as the cells accumulated Na by diffusion from the external solution. An applied potential would, in this model, affect the diffusional entry step but not the electrically neutral active step. Therefore, a hyperpolarizing PD would slow the rate of Na entry (and thereby slow transport) and a depolarizing PD would accelerate entry until the cells accumulated sufficient Na to saturate the active transport step. The rate of transport would, therefore, show an increase as the potential was increased in the depolarizing direction until it saturated, displaying S-shaped characteristics. At two different external Na concentrations, the rate of transport would be expected to reach the *same* level of saturation, but the PDs at which saturation was reached would be different. This predicted behavior is clearly different from that observed (Fig. 4), where *different* saturation levels are reached at different concentrations.

Thus, the present results suggest that the initial entry of Na into the skin is not due to simple diffusion. Similar conclusions have been reached on the basis of indirect evidence in both frog skin and toad bladder, and recent reports (20, 21) of direct measurements of the entry of Na into frog skin have confirmed this point directly. These studies have shown that at least a large portion of the unidirectional Na flux from the outside solution into the skin is mediated by a process that saturates as a function of external Na concentration. This Na influx process is competitively inhibited by Li (21) and is also inhibited by K in the external solution (20). On the basis of these observations, saturation of transepithelial Na transport as a function of external Na concentration and the competitive inhibition of this process by K appear to be properties of the entry process rather than of a Na pump located in the inner portion of the epithelium.

In view of these considerations, it seems appropriate to inquire whether or not the effects of PD on Na transport could also involve the system for mediated Na transfer across this outer barrier. Although the relative independence of the effects of external Na concentration and PD requires that the interaction between Na and sites in the outer barrier be voltage insensitive, once a Na ion is adsorbed on the surface, its rate of movement through the barrier could be voltage dependent. This type of process could be modelled by a voltage-sensitive carrier or by charged mobile sites within the barrier. In the carrier model illustrated in Fig. 9, external Na interacts with a carrier (neutral for the sake of argument), forming a positively charged complex that is translocated in a voltage-dependent step to the inside surface of the barrier. If the carrier were negatively charged, it would form a neutral complex with Na;

the voltage-dependent step would be, in this case, the return of the charged carrier. In the model with charged mobile sites, external Na would interact with Na-selective sites from which it would diffuse through Na-selective charged channels to the internal surface. The voltage sensitivity of the translocation step would arise from the distribution of mobile sites within the barrier as a function of potential (22, 23). These models are phenomenologically indistinguishable at present and have identical mathematical descriptions; we shall discuss only the carrier model.

A mathematical description of the carrier model is presented in Appendix I. Starting with the assumption that the charged carrier-ion complex moves through a constant electric field across the membrane, it is shown that, under

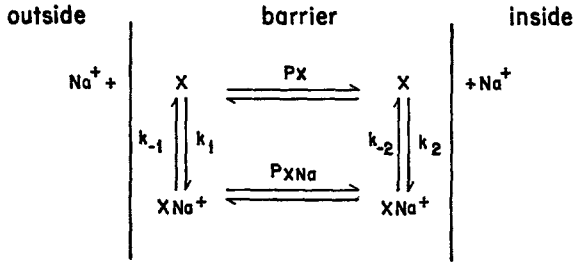

FIGURE 9. Voltage-sensitive carrier model for Na transport. See text for details.

specific simplifying conditions discussed below, the Na flux may be described by

$$J_{Na}^{i(o)} = c_T P_X \left[\frac{f(V)}{K_X + f(V)}\right]\left[\frac{c_{Na}}{c_{Na} + K_T \dfrac{f(V)}{K_X + f(V)}}\right], \tag{3}$$

where

$$f(V) = \frac{FV/RT}{\exp\left(\dfrac{FV}{RT}\right) - 1}, \tag{4}$$

$$K_X = \frac{P_X}{P_{XNa}}, \tag{5}$$

$$K_T = \frac{2P_X}{k_1}, \tag{6}$$

c_T is proportional to the total carrier concentration in the membrane, P_X and P_{XNa} are the permeabilities of the uncomplexed and complexed carriers, respectively, and k_1 is the carrier-ion association rate on the outside surface. Plots of theoretical $J_{Na}^{i(o)}$ vs. PD as predicted by Eq. 3 are shown in Fig. 10 for several external Na concentrations. The qualitative behavior is similar to the

experimental data, demonstrating S-shaped characteristics as a function of potential, and saturation as a function of external Na concentration.

The main assumption made in deriving Eq. 3 is that the rates of carrier-ion association be very different on the two sides of the membrane, favoring association on the external surface and dissociation on the internal surface. The actual assumption is that $k_1, k_{-2} \gg k_{-1}, k_2$, where 1 and 2 refer to the outside and inside surfaces, respectively. The result is an equation in which the effect of applied potential may be clearly separated from the effect of external Na concentration. The first term in brackets is responsible for the S-shaped characteristics; it is written as a general function of voltage to empha-

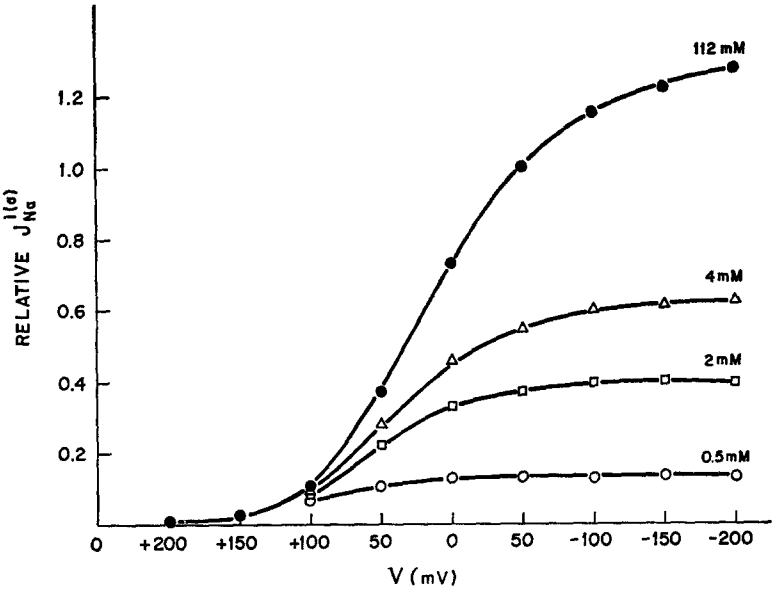

FIGURE 10. Theoretical $J_{Na}^{(a)i}$ vs. PD curves based on the model shown in Fig. 9; calculated from Eq. A 12. $K_X = 1$, $K_T = 5$.

size that the S-shape could be obtained from many similar functions. The particular form of $f(V)$ used was derived from the constant field assumption; however, assuming a linear carrier concentration gradient and an exponential voltage drop across the barrier would result in a different $f(V)$ (22) that would also yield an S-shaped curve. The exact shape of the curve depends on $f(V)$ and, therefore, on the potential and carrier concentration distributions within the barrier. The magnitude of K_X determines the range of PD in which saturation is reached; in Fig. 10 we assumed that $K_X = 1.0$ or that $P_{XNa} = P_X$. If only a constant fraction of the applied PD appears across the barrier of interest the theoretical curves would have the same shape as those shown in Fig. 10. The second term in brackets represents the saturation obtained as

the external Na concentration is increased. The half-saturation concentration is potential dependent, increasing with increase in depolarizing potential; this factor results in saturation at lower PD the lower the external Na concentration which mimics the experimental data (Fig. 4). A dependence of the half-saturation concentration on PD is shown in Fig. 6 *a* for the range 0 to −50 mV but not in Fig. 6 *b* for the 50 mV to 0 range. The reason for this discrepancy is unknown, but it might point to a deficiency in the model at hyperpolarizing potentials, possibly because the assumptions are less valid under those conditions. Also, the theoretical curves do not represent the experimental data as well at hyperpolarizing potentials as at depolarizing ones. Nonetheless, the predicted effects of PD on maximal flux rate agree well with those observed (Fig. 6). The predicted ratio of maximal flux at 50 mV to that at zero PD is 0.48 and the observed ratio is 0.41. At −50 mV, the predicted and observed ratios are 1.4 and 1.5, respectively. Thus, the model, even in its simple form, provides a good qualitative fit to the experimental data both as a function of potential and external Na concentration.

These considerations indicate that the present results could be explained qualitatively by properties of a single barrier containing a mediated, voltage-sensitive transfer system for Na (that could be active or passive). They do not, however, rule out more complex systems involving two (or more) barriers in series. For example, one can conceive of a Na entry step that is passive but mediated by a system such as that shown in Fig. 9 coupled with an active, electroneutral extrusion mechanism at an inner barrier. As indicated by the analysis in Appendix II, and as shown in Fig. 11, such a system will also display saturation with PD. If the neutral step is at least as fast as the entry step, the calculated curves fit the observed data as well as those shown in Fig. 10 for the single-barrier model. The data could probably also be fit by a model involving a mediated but voltage-insensitive entry step (such as Na-H exchange [24]) and an electrogenic extrusion mechanism. However, the observations of Biber and Saunders (25) that the Na entry into the skin is voltage sensitive would tend to rule out the simple form of such a model.

The bulk of the information now available on Na transport across frog skin appears to favor a system involving at least two barriers in a series array although the exact nature of these barriers and their anatomical location remains somewhat uncertain. The data on these points has been reviewed and discussed by several authors (see for example Erlij [26]) and need not be repeated. On the other hand, Cereijido and his co-workers (27) have suggested that Na transport in frog skin may involve a process that is equivalent to only a single barrier in that transported Na does not actually enter the cells of the epithelium. In addition, Biber (28) has reported that entry of Na into the skin across the outer surface is sensitive to metabolic inhibition and to ouabain, suggesting that this process may have certain characteristics usually

associated with an active step. Such a behavior might be viewed as consistent with the hypothesis advanced by Cereijido. The qualitative conclusion that our results could be explained by properties of a single barrier suggest that they could be consistent with Cereijido's hypothesis. On the other hand, the results are equally consistent with at least some versions of the more classical

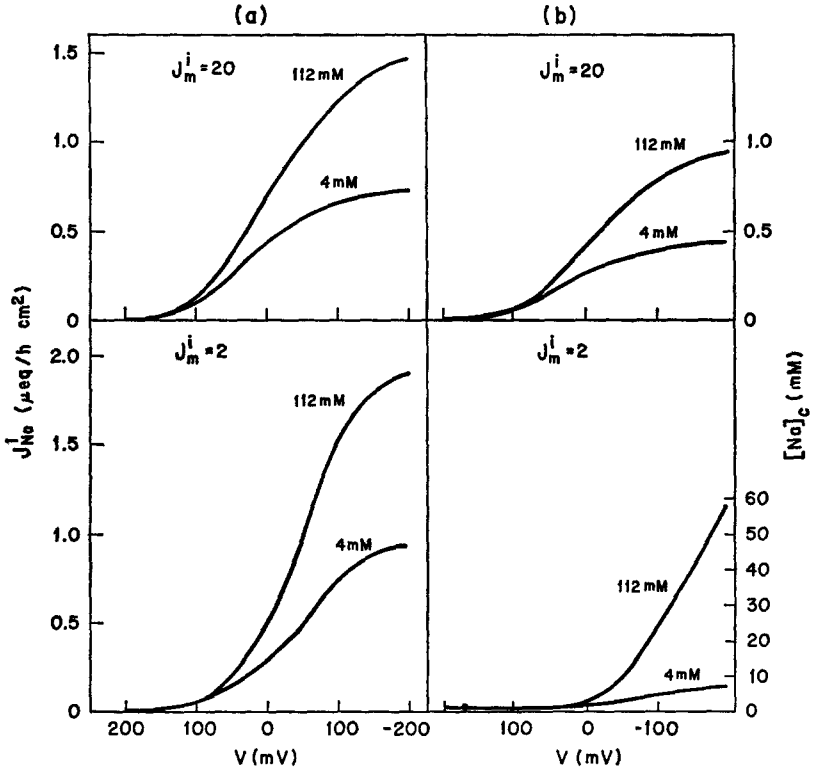

FIGURE 11. Theoretical curves based on the two-barrier model described in Appendix II. Calculated using $J_m^i = 20$ and 2, $C_T P_X = 2$, $K_X = 1$, $K_T = K'_T = 5$, $K_i = 10$. (*a*) J_{Na}^i vs. PD, (*b*) $[Na]_c$ vs. PD. (Notice the different scales on the right-hand side for $[Na]_c$.)

two-barrier hypothesis and they do not, at this stage, permit distinction between the mechanisms. In this respect, it is of interest to note that under the conditions best replicating the experimental results, the two-barrier system involves a very small "transport pool" for Na. The top portion of Fig. 11 shows that the calculated Na concentration in the transport pool remains under 1 mM at all PDs, a value that represents less than 5% of the cellular Na concentration in the epithelium (29). A transport pool of this size would not be easily detected and the calculation suggests that a very small transport pool cannot be taken as firm evidence against a two-barrier system. However, both

the single-barrier and dual-barrier models discussed are of qualitative value only because the analyses are oversimplified. For example, we have implicitly assumed that all of the imposed PD appears across the barrier, and we have ignored such factors as possible changes in cell volume and in cellular ion concentrations and the existence of nonsteady states. Thus a number of questions remain to be answered before the effects of PD on Na transport in frog skin are fully understood and can be correlated with the morphological characteristics of the epithelium.

APPENDIX I

A Single-Barrier Model

Under steady-state conditions, the system shown in Fig. 9 can be described by the following set of equations:

$$\frac{dc_x}{dt} = -k_1 c_X c_{Na} + k_{-1} c_{XNa} + P_X c'_X - P_X c_X = 0 \qquad (A1)$$

$$\frac{dc_{XNa}}{dt} = -k_{-1} c_{XNa} + k_1 c_X c_{Na} + P_{-1} c'_{XNa} - P_1 c_{XNa} = 0 \qquad (A2)$$

$$\frac{dc'_{XNa}}{dt} = -k_{-2} c'_{XNa} + k_2 c'_X c'_{Na} + P_1 c_{XNa} - P_{-1} c'_{XNa} = 0 \qquad (A3)$$

$$\frac{dc'_X}{dt} = -k_2 c'_X c'_{Na} + k_{-2} c'_{XNa} + P_X c_X - P_X c'_X = 0 \qquad (A4)$$

in which k represents rate coefficient and the c concentration. If the flux of $X\text{Na}^+$ is assumed to be described by the Goldman "constant field" equation,

$$P_1 = \frac{P_{XNa}\left(\frac{VF}{RT}\right)}{\exp\left(\frac{VF}{RT}\right) - 1} \quad \text{and} \quad P_{-1} = \frac{P_{XNa}\left(\frac{VF}{RT}\right)\exp\left(\frac{VF}{RT}\right)}{\exp\left(\frac{VF}{RT}\right) - 1},$$

in which V is the potential across the barrier. Conservation of total carrier requires that

$$c_T = c_X + c_{XNa} + c'_X + c'_{XNa} \qquad (A5)$$

From these expressions, we wish to evaluate the unidirectional "influx" $J^{i(a)}$.

To calculate the influx in a general way, we must determine the rate of tracer appearance at the inner side of the membrane assuming that negligible tracer is present on that side. This quantity, J^{i*} is given by

$$J^{i*} = k_{-2} c'_{XNa*} \qquad (A6)$$

in which the asterisk denotes the tracer. Equations analogous to Eq. A 2 and A 3 can

be written for c_{XNa^*} and c'_{XNa^*} keeping in mind that $c'_{Na^*} = 0$. These expressions may be solved for c'_{XNa^*} to yield

$$c'_{XNa^*} = \frac{P_1 k_1 c_X c_{Na^*}}{k_{-1}k_{-2} + k_{-1}P_{-1} + k_{-2}P_1}. \tag{A 7}$$

By the usual assumption regarding tracer behavior, total influx, $J^{i(a)}$, is given by

$$J^{i(a)} = J^{i*}[c_{Na}/c_{Na^*}]. \tag{A 8}$$

Introducing Eq. A 7 into Eq. A 6, and the resulting expression into Eq. A 8, we obtain

$$J^{i(a)} = \frac{P_1 k_1 k_{-2} c_X c_{Na}}{k_{-1}k_{-2} + k_{-1}P_{-1} + k_{-2}P_1}. \tag{A 9}$$

J^i can now be evaluated by solving Eq. A 1, A 2, A 5, and A 7 simultaneously for c_X and introducing it into Eq. A 9. We shall not present the general result which is unwieldy, but shall assume that k_{-1} and k_2 are very much smaller than k_1 and k_{-2}. Under these conditions, Eq. A 9 becomes simply

$$J^{i(a)} = k_1 c_X c_{Na} \tag{A 10}$$

and

$$c_X = \frac{c_T P_1 P_X k_{-2}}{k_1 c_{Na}[k_{-2}(P_1 + P_X) + P_X(P_1 + P_{-1})] + 2k_{-2}P_1P_X}. \tag{A 11}$$

If we assume for simplicity that $k_{-2}(P_1 + P_X) \gg P_X(P_1 + P_{-1})$, J^i becomes

$$J^{i(a)} = c_T P_X \left(\frac{f(V)}{K_X + f(V)}\right)\left(\frac{c_{Na}}{c_{Na} + K_T \dfrac{f(V)}{K_X + f(V)}}\right) \tag{A 12}$$

in which

$$f(V) = \frac{FV/RT}{\exp(FV/RT) - 1}; \qquad K_X = P_X/P_{XNa}; \qquad K_T = 2P_X/k_1.$$

The behavior of Eq. A 12 is discussed in the text.

The assumptions used to obtain Eq. A 12 are not as restrictive as may appear at first sight. They provide a particularly simple expression for J^i but the general expression should behave in a qualitatively similar manner. Although the general equation is much more complex, the two voltage-dependent portions have the form $[a + a'f(V)]/[b + b'f(V)]$ at high-depolarizing potentials and hence will saturate under these conditions as do the simpler terms in Eq. A 12.

APPENDIX II

A Two-Barrier Model

We assume that the outer barrier contains a system of the type shown in Fig. 9 whose properties are essentially those discussed in Appendix I. Net Na flux (J^0_{Na}) across this

barrier will be given by

$$J^0_{Na} = \frac{J^0_m [Na]_0}{K_0 + [Na]_0} - \frac{J^{0'}_m [Na]_c}{K'_0 + [Na]_c}, \tag{A 13}$$

in which

$$J^0_m = c_T P_X \left(\frac{f(V)}{K_X + f(V)}\right), \qquad K_0 = K_T \left(\frac{f(V)}{K_X + f(V)}\right),$$

$$J^{0'}_m = c_T P_X \left(\frac{f'(V)}{K_X + f'(V)}\right), \qquad K'_0 = K'_T \left(\frac{f'(V)}{K_X + f'(V)}\right),$$

where $f(V)$ is taken as given in Appendix I and $f'(V) = f(V) \exp [FV/RT]$. The inner barrier is assumed to contain a neutral active transport system that is irreversible so that net Na flux (J^i_{Na}) is given simply by

$$J^i_{Na} = \frac{J^i_m [Na]_c}{K_i + [Na]_c}. \tag{A 14}$$

If we assume that there is no other mechanism for Na to cross the inner barrier, unidirectional Na flux from outside to inside will also be given by Eq. A 14. If the system is in a steady state,

$$J^0_{Na} = J^i_{Na} \tag{A 15}$$

Eq. A 13 and A 14 can be introduced into Eq. A 15 and the resulting expression solved for $[Na]_c$ yielding

$$\begin{aligned}&[Na]_c^2\{J^0_m[Na]_0 - (J^{0'}_m + J^i_m)(K_0 + [Na]_0)\}\\ &+ [Na]_c\{J^0_m[Na]_0(K'_0 + K_i) - (K_0 + [Na]_0)(J^{0'}_m K_i + J^i_m K'_0)\}\\ &+ J^0_m K'_0 K_i [Na]_0 = 0.\end{aligned} \tag{A 16}$$

This expression can be used to evaluate $[Na]_c$ at various values of $[Na]_0$, PD, and J^i_m; Na flux can then be calculated from Eq. A 14. Some results are shown in Fig. 11. When $J^i_m = 20$, $J^i_m > J^0_m$ at all PDs, and the J^i_{Na} vs. PD curves (Fig. 11 *a*) are almost identical to those in Fig. 10 because they reflect the properties of the entry step. The $[Na]_c$, shown in Fig. 11 *b*, follows a similar pattern with PD as J^i_{Na}, always remaining below 1 mM. At $J^i_m = 2$, $J^i_m \approx J^0_m$, and the theoretical curves still qualitatively fit the data; however, at high-depolarizing PDs, $[Na]_c$ increases rapidly at 112 mM. If $J^i_m < J^0_m$ at high-depolarizing potentials, the steady-state requirement (Eq. A 15) cannot be met unless $[Na]_0$ is quite small because $J^{0'}_m \to 0$ under these conditions and the above analysis is no longer tenable. Thus, this relatively simplified two-barrier model has a limited range of validity at least for describing effects of applied PD.

We are indebted to Miss Anne Lamont for valuable technical assistance.
This work was supported by United States Public Health Service Research Grant AM-12028 from the National Institute of Arthritis, Metabolism and Digestive Diseases.

Dr. Mandel was supported by United States Public Health Service Postdoctoral Fellowship AM-45037 from the National Institute of Arthritis, Metabolism and Digestive Diseases.

Received for publication 16 November 1972.

REFERENCES

1. USSING, H. H., and K. ZERAHN. 1950. Active transport of sodium as the source of electric current in the short-circuited isolated frog skin. *Acta Physiol. Scand.* **23**:110.
2. FINKELSTEIN, A. 1964. Electrical excitability of isolated frog skin and toad bladder. *J. Gen. Physiol.* **47**:545.
3. FISHMAN, H. M., and R. I. MACEY. 1969. The N-shaped current-potential characteristic in frog skin. I. Time development during step voltage clamp. *Biophys. J.* **9**:127.
4. CANDIA, O. A. 1970. The hyperpolarizing region of the current-voltage curve in frog skin. *Biophys. J.* **10**:323.
5. CIVAN, M. M. 1970. Effects of active sodium transport on current-voltage relationship of toad bladder. *Am. J. Physiol.* **219**:234.
6. VIEIRA, F. L., S. R. CAPLAN, and A. ESSIG. 1972. Energetics of sodium transport in frog skin. II. The effects of electrical potential on oxygen consumption. *J. Gen. Physiol.* **59**:77.
7. NELLANS, H. 1971. Oxygen consumption and active sodium transport in the toad bladder. Ph.D. Thesis. Yale University, New Haven.
8. BRINLEY, F. J., and L. J. MULLINS. 1971. The fluxes of sodium and potassium across the squid axon membrane under conditions of altered membrane potential. *Fed. Proc.* **30**:255.
9. THOMAS, R. C. 1972. Intracellular sodium activity and the sodium pump in snail neurones. *J. Physiol. (Lond.).* **220**:55.
10. MANDEL, L. J., and P. F. CURRAN. 1972. Response of the frog skin to steady-state voltage clamping. I. The shunt pathway. *J. Gen. Physiol.* **59**:503.
11. FRIZZELL, R. A., and S. G. SCHULTZ. 1972. Ionic conductances of extracellular shunt pathway in rabbit ileum. Influence of shunt on transmural sodium transport and electrical potential differences. *J. Gen. Physiol.* **59**:318.
12. MACROBBIE, E. A. C., and H. H. USSING. 1961. Osmotic behaviour of the epithelial cells of frog skin. *Acta Physiol. Scand.* **53**:348.
13. USSING, H. H. 1960. The frog skin potential. *J. Gen. Physiol.* **43**(5, Suppl.):135s.
14. BIBER, T. U. L., R. A. CHEZ, and P. F. CURRAN. 1966. Na transport across frog skin at low external Na concentrations. *J. Gen. Physiol.* **49**:1161.
15. CEREIJIDO, M., F. HERRERA, W. J. FLANIGAN, and P. F. CURRAN. 1964. The influence of Na concentration of Na transport across frog skin. *J. Gen. Physiol.* **47**:879.
16. DELAHAY, P. 1965. Double layer and electrode kinetics. John Wiley and Sons, Inc., New York.
17. SZABO, G., G. EISENMAN, and S. CIANI. 1969. The effects of the macrotetralide actin antibiotics on the electrical properties of phospholipid bilayer membranes. *J. Membrane Biol.* **1**:346.
18. KOEFOED-JOHNSEN, V., and H. H. Ussing. 1958. The nature of the frog skin potential. *Acta Physiol. Scand.* **42**:298.
19. USSING, H. H. 1967. Active sodium transport across the frog skin epithelium and its relation to epithelial structure. *Ber. Bunsenges. Phys. Chem.* **71**:807.
20. ROTUNNO, C. A., F. A. VILALLONGA, M. FERNANDEZ, and M. CEREIJIDO. 1970. The penetration of sodium into the epithelium of the frog skin. *J. Gen. Physiol.* **55**:716.
21. BIBER, T. U. L., and P. F. CURRAN. 1970. Direct measurement of uptake of sodium at the outer surface of the frog skin. *J. Gen. Physiol.* **56**:83.
22. CONTI, F., and G. EISENMAN. 1966. The steady-state properties of an ion exchange membrane with mobile sites. *Biophys. J.* **6**:227.
23. WALKER, J. L., JR., and G. EISENMAN. 1966. A test of the theory of the steady-state properties of an ion exchange membrane with mobile sites and dissociated counterions. *Biophys. J.* **6**:513.

24. GARCÍA ROMEU, F., A. SALIBIÁN, and S. PEZZANI-HERNÁNDEZ. 1969. The nature of the *in vivo* sodium and chloride uptake mechanisms through the epithelium of the Chilean frog *Calyptocephalella gayi*. *J. Gen. Physiol.* **53**:816.
25. BIBER, T. U. L., and M. L. SANDERS. 1973. Influence of transepithelial potential difference on solution uptake at the outer surface of the isolated frog skin. *J. Gen. Physiol.* **61**:529.
26. ERLIJ, D. 1971. Salt transport across isolated Frog skin. *Philos. Trans. R. Soc. Lond. Ser. B Biol. Sci.* **262**:153.
27. CEREIJIDO, M., and C. A. ROTUNNO. 1968. Fluxes and distribution of sodium in frog skin: a new model. *J. Gen. Physiol.* **51**(5, Pt. 2):280s.
28. BIBER, T. U. L. 1971. Effect of changes in transepithelial transport on the uptake of sodium across the outer surface of frog skin. *J. Gen. Physiol.* **58**:131.
29. ACEVES, J., and D. ERLIJ. 1971. Sodium transport across the isolated epithelium of the frog skin. *J. Physiol. (Lond.)*. **212**:195.